Available online at www.sciencedirect.com
ScienceDirect
Journal of Computational and Applied Mathematics 215 (2008) 547–556
JOURNAL OF COMPUTATIONAL AND APPLIED MATHEMATICS
www.elsevier.com/locate/cam

On uniformly high-order accurate residual distribution schemes for advection–diffusion

M. Ricchiuto[a,*], N. Villedieu[c], R. Abgrall[a,b], H. Deconinck[c]

[a] *INRIA Futurs, project ScAlApplix and Mathématiques Appliquées de Bordeaux, Université de Bordeaux I, 351 cours de la Libération, 33405 Talence cedex, France*
[b] *Institut Universitaire de France, France*
[c] *Department of Aeronautics and aerospace, von Karman Institute for Fluid Dynamics, Chaussée de Waterloo 72, B-1640 Rhode-Saint-Genèse, Belgium*

Received 17 July 2005

Abstract

We discuss preliminary results on the construction of uniformly high-order residual distribution ($\mathscr{RD}$) type discretizations for steady advection–diffusion on unstructured grids. A properly designed scaling of the $\mathscr{RD}$ upwind stabilization with the physical viscosity allows to obtain schemes with uniform and arbitrary accuracy, on a very compact stencil. Second and third-order examples are given to illustrate the potential of the approach.

MSC: 65M60; 65M99

Keywords: Advection–diffusion; Residual distribution; Very high-order schemes; Compact schemes

1. Problem setting

We consider the numerical solution of the steady limit of the scalar advection–diffusion equation

$$\frac{\partial u}{\partial t} + \vec{a} \cdot \nabla u = \nabla \cdot (\nu \nabla u) \quad \text{on } \Omega \subset \mathbb{R}^2 \tag{1.1}$$

on an unstructured triangulation of the spatial domain Ω, denoted by τ_h, with h a characteristic element size (e.g., largest element diameter). Given the nodal values $\{u_i\}_{i\in\tau_h}$, we denote by u_h the kth order continuous polynomial approximation obtained as

$$u_h = \sum_{i\in\tau_h} \psi_i(x, y) u_i$$

with $\psi_i(x, y)$ the continuous Lagrangian basis functions on τ_h. The piecewise linear P^1 basis functions are denoted by $\varphi_i(x, y)$. Given a P^k Lagrangian element T, with $k \geqslant 1$, consider its P^1 conformal sub-triangulation, and denote by

* Corresponding author. Tel.: +33 5 40 00 37 94; fax: +33 5 40 00 38 95.
E-mail address: Mario.Ricchiuto@inria.fr (M. Ricchiuto).

0377-0427/$ - see front matter © 2007 Elsevier B.V. All rights reserved.
doi:10.1016/j.cam.2006.03.059

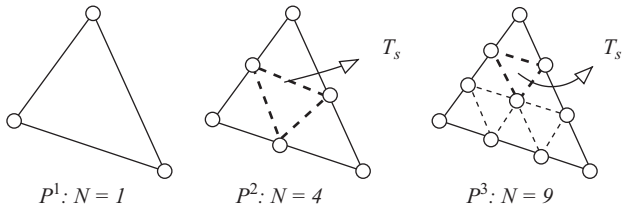

Fig. 1. Sub-triangulations of Lagrangian elements.

$\{T_s\}_{s=1,N}$ the sub-elements in T, as in Fig. 1. We consider cell-vertex schemes for which the discrete analog of (1.1) reads

$$u_i^{n+1} = u_i^n - \delta_i \sum_{T|i\in T} \sum_{T_s\in T} \Psi_i^{T_s} \tag{1.2}$$

with δ_i an iteration parameter. In the case $\nu = 0$, the local nodal residuals $\Psi_i^{T_s}$ satisfy

$$\sum_{j\in T_s} \Psi_j^{T_s} = \phi^{T_s} = \int_{T_s} \vec{a}\cdot\nabla u_h \,\mathrm{d}x\,\mathrm{d}y$$

giving back the fluctuation schemes of [1]. We want to extend these schemes to the solution of (1.1), in a way guaranteeing uniform $(k+1)$th order accuracy on a given P^k triangulation.

2. Second order advection–diffusion: the P^1 case

For a linear P^1 interpolation and pure advection, the schemes of [1] reduce to the well-known residual distribution ($\mathscr{RD}$) schemes [2]. On $T \in \tau_h$, the nodal residuals Ψ_i^T are computed as

$$\Psi_i^T = \beta_i \phi^T, \quad \phi^T = \int_T \vec{a}\cdot\nabla u_h \,\mathrm{d}x\,\mathrm{d}y, \quad \sum_{j\in T} \beta_j = 1, \tag{2.1}$$

where the coefficients β_i define a particular distribution scheme [2]. The extension of $\mathscr{RD}$ schemes to the solution of (1.1) is often achieved by invoking an equivalence with finite elements (FE) Petrov–Galerkin ($\mathscr{PG}$) schemes [6], and discretizing the diffusion operator with a standard Galerkin approach, leading to

$$\Psi_i^T = \beta_i \phi^T + \int_T \nu\nabla\varphi_i\cdot\nabla u_h \,\mathrm{d}x\,\mathrm{d}y. \tag{2.2}$$

2.1. $\mathscr{PG}$ formulation with bubble function

The $\mathscr{PG}$ analogies presented in literature [2] do not really lend themselves to the approximation of (1.1), due to use of *discontinuous* test functions. Here, we consider the $\mathscr{PG}$ weak formulation

$$\Psi_i^T = \int_T \omega_i \vec{a}\cdot\nabla u_h \,\mathrm{d}x\,\mathrm{d}y + \int_T \nu\nabla\omega_i\cdot\nabla u_h \,\mathrm{d}x\,\mathrm{d}y$$

with the following set of *continuous* test functions

$$\omega_i = \varphi_i + s_i(x,y), \quad s_i(x,y) = \sum_{T\in\tau_h} \chi^T(x,y)(3\beta_i - 1)s^T(x,y) \tag{2.3}$$

with s^T the piecewise linear *bubble*, which is zero on the boundary of T and one in its gravity center (Fig. 2), and $\chi^T(x,y)$ the characteristic function of element T: $\chi^T(x,y) = 1$ if $(x,y)\in T$, and zero otherwise. One can check that, for constant advection speed, (2.3) reduces to (2.2). In this $\mathscr{PG}$ formulation of $\mathscr{RD}$, shape and test functions belong to the same functional space $H_0^1(\Omega)$, the natural space in which to seek solutions of (1.1).

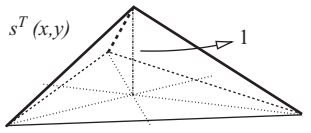

Fig. 2. Piecewise linear *bubble* function.

This $\mathscr{PG}$ formulation is mathematically better posed. However, it still suffers from a lack of uniform (with h) accuracy, due to the fact that the discrete advection and diffusion operators are not consistently coupled. Note that the former always introduces some stabilization, generally in the form of upwinding. As pointed out in [5], in the major literature on $\mathscr{RD}$ this issue has never been analyzed, even though well known in the FE framework. In particular, in stabilized FE schemes this is taken care of through the introduction of a proper scaling of the streamline dissipation [4,3]. Here we propose a similar approach. Defining on $T \in \tau_h$ the Peclet number

$$Pe = \frac{h\sqrt{\vec{a}\cdot\vec{a}}}{\nu}$$

we modify (2.3) by redefining the perturbation $s_i(x, y)$ as [4,3]

$$s_i(x, y) = \sum_{T\in\tau_h} \chi^T(x, y)\xi(Pe)(3\beta_i - 1)s^T(x, y), \quad \xi(Pe) = \min(1, Pe). \tag{2.4}$$

As h is refined, the stabilization introduced in the discrete advection operator is reduced, ultimately leading to a pure Galerkin scheme in the diffusion dominated regime. As we will shortly show, this simple modification allows to obtain uniform second-order accuracy. Note that this leads to the $\mathscr{RD}$ scheme with local nodal residuals

$$\Psi_i^T = \beta_i^* \phi^T + \int_T \nu\nabla\varphi_i \cdot \nabla u_h \,\mathrm{d}x\,\mathrm{d}y, \quad \beta_i^* = \frac{1}{3} + \xi(Pe)\left(\beta_i - \frac{1}{3}\right). \tag{2.5}$$

2.2. Numerical experiments

On the spatial domain $[0, 1]^2$ we consider the set of problems admitting the exact solution [5]

$$u = -\cos(2\pi\eta)\,\exp\left(\frac{\zeta(1-\sqrt{1+16\pi^2\nu^2})}{2\nu}\right),$$

where $\eta = \vec{a}_y x - \vec{a}_x y$ and $\zeta = \vec{a}_x x + \vec{a}_y y$. Here we consider the case $\vec{a} = (a_x, a_y) = (0, 1)$. We perform a grid convergence study using (2.2) and (2.5), with the distribution coefficients β_i corresponding to the multidimensional upwind LDA scheme [2]:

$$\beta_i = \frac{\max(0, \vec{a}\cdot\vec{n}_i)}{\sum_{j\in T}\max(0, \vec{a}\cdot\vec{n}_j)} \tag{2.6}$$

with $\vec{n}_j$ the inward pointing vector, normal to the edge of T opposite to node j, scaled by the length of the edge. We refer to LDA* scheme as to the one obtained by using (2.5) in (1.2), and to LDA scheme as to the one obtained using (2.2). The study is performed on six unstructured triangulations, obtained with a Weatherhill algorithm, with h from 0.1 to 3.125×10^{-3}. We discuss the results obtained for $\nu = 0.01$ (corresponding to $Pe \in [0.625, 10]$), however, similar results have been obtained for values of ν from 10^{-6} to 1. On the left in Fig. 3, we plot the grid convergence of the L^2 norm of the error for the LDA and LDA* schemes. As in [5], the figure clearly shows the loss of accuracy of the LDA scheme when the *Pe* number decreases. The simple modification (2.5) restores the uniform accuracy, leading to a truly second-order discretization. Moreover, as shown by the plot on the right picture in Fig. 3, the LDA* scheme also gives a consistent and uniform first-order accurate prediction of ∇u.

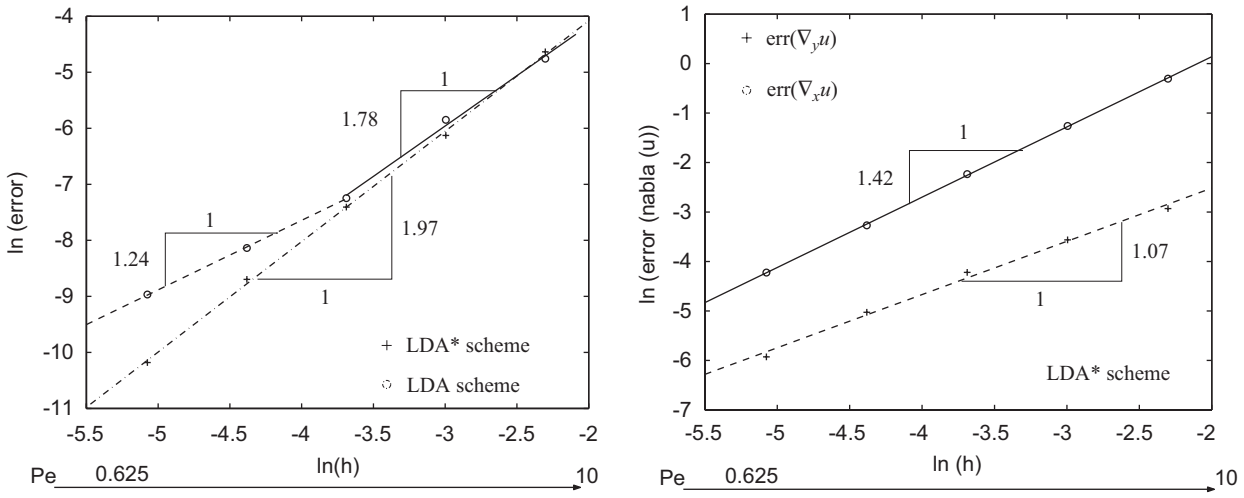

Fig. 3. Grid convergence study: $\nu = 0.01$. Error in terms of u (left) and of ∇u (right).

3. Generalization to $k > 1$

We give one possible generalization of the construction to P^k elements, with $k \geqslant 2$. We define, on $T_s \in T \in \tau_h$, the continuous *bubble* functions $s^{T_s}(x, y)$ displayed in Fig. 4 for $k = 2,\ 3$. As in the P^1 case, $s^{T_s}(x, y)$ is zero on ∂T_s and outside T_s, while it is one in its gravity center. Compared to the shape functions $\{\psi_j\}_{j\in T}$, the local regularity (within T) of these functions is quite low. However, ultimately both shape and bubble functions are in the same functional space $H_0^1(\Omega)$ and share simple C^0 continuity. More complex definitions of these bubbles are possible, and the ideas presented in the paper can be used in conjunction with these definitions. We now devise $\mathscr{RD}$ flavored $\mathscr{PG}$ approximations to (1.1).

Given a fluctuation scheme with distribution coefficient β_i, a first approach is to consider the $\mathscr{PG}$ schemes with test functions

$$\omega_i(x, y) = \psi_i(x, y) + s_i(x, y), \quad s_i(x, y) = \sum_{T|i\in T} \sum_{T_s\in T} \chi^{T_s}(x, y)\alpha_i^{T_s} s^{T_s}(x, y), \tag{3.1}$$

where the constant $\alpha_i^{T_s}$ is determined such that for a piecewise linear solution one gets back a $\mathscr{RD}$ scheme with distribution coefficient β_i in all the sub-elements T_s containing the node:

$$\frac{1}{|T_s|}\int_{T_s} \omega_i \,\mathrm{d}x\,\mathrm{d}y = \begin{cases} \beta_i & \text{if } i \in T_s, \\ 0 & \text{if } i \notin T_s. \end{cases} \tag{3.2}$$

Scheme $\mathscr{PG}^1(P^2)$*-LDA*: The $\mathscr{PG}$ discrete analog of (1.1) then becomes

$$\begin{aligned} &\int_\Omega \omega_i \vec{a}\cdot\nabla u_h \,\mathrm{d}x\,\mathrm{d}y + \int_\Omega \nu\nabla\omega_i\cdot\nabla u_h \,\mathrm{d}x\,\mathrm{d}y \\ &= \sum_{T|i\in T}\sum_{T_s\in T}\left\{\int_{T_s} \omega_i\vec{a}\cdot\nabla u_h \,\mathrm{d}x\,\mathrm{d}y + \int_{T_s}\nu\nabla\omega_i\cdot\nabla u_h \,\mathrm{d}x\,\mathrm{d}y\right\} = 0 \quad \forall i \in \tau_h. \end{aligned} \tag{3.3}$$

For $T \in \tau_h$, with $i \in T$, last expression involves all the sub-elements of T and not only the ones containing node i. Hence, it is somehow more complex than the fluctuation approach of [1], in which only the sub-elements containing i are used in (1.2). A construction leading to such a compact scheme is achieved by considering test functions obtained by perturbing the P^1 basis functions on the conformal sub-triangulation, which we still denote by $\{\varphi_i\}_{i\in\tau_h}$ (see Fig. 5).

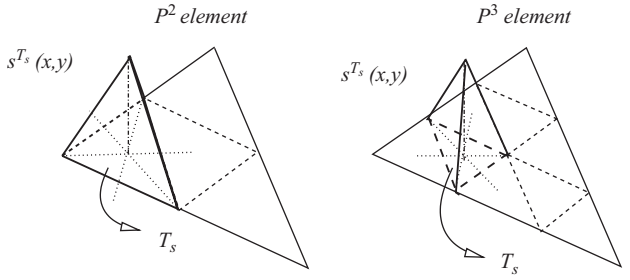

Fig. 4. Piecewise linear *bubble* functions: P^2 and P^3 elements.

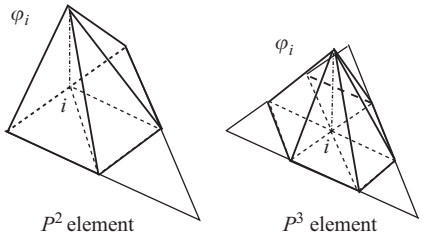

Fig. 5. Piecewise linear basis functions on the sub-elements.

In particular, we consider the $\mathscr{PG}$ scheme with test functions

$$\widetilde{\omega}_i(x,y) = \varphi_i(x,y) + \widetilde{s}_i(x,y), \quad \widetilde{s}_i = \sum_{T_s | i \in T_s} \chi^{T_s}(x,y)(3\beta_i - 1)s^{T_s}(x,y). \tag{3.4}$$

As before, we note that $\widetilde{\omega}_i$ satisfies by construction

$$\frac{1}{|T_s|}\int_{T_s} \widetilde{\omega}_i \,\mathrm{d}x\,\mathrm{d}y = \beta_i.$$

Scheme $\mathscr{PG}^2(P^2)$*-LDA*: The $\mathscr{PG}$ discrete analog of (1.1) then becomes

$$\begin{aligned}&\int_\Omega \widetilde{\omega}_i \vec{a}\cdot\nabla u_h \,\mathrm{d}x\,\mathrm{d}y + \int_\Omega \nu\nabla\widetilde{\omega}_i\cdot\nabla u_h \,\mathrm{d}x\,\mathrm{d}y\\ &\quad= \sum_{T_s \,|\, i\in T_s}\left\{\int_{T_s}\widetilde{\omega}_i\vec{a}\cdot\nabla u_h\,\mathrm{d}x\,\mathrm{d}y + \int_{T_s}\nu\nabla\widetilde{\omega}_i\cdot\nabla u_h\,\mathrm{d}x\,\mathrm{d}y\right\} = 0 \quad \forall i\in\tau_h\end{aligned} \tag{3.5}$$

which is considerably more compact and computationally convenient than (3.3). This scheme is not a standard $\mathscr{PG}$ discretization, as the test functions are obtained by perturbing basis functions different from the ones defining u_h. A theoretical justification of this approach will be reported in a forthcoming publication. Here, its accuracy will be proven by the numerical results. (3.5) still does not represent a generalization of the fluctuation approach of [1]. Moreover, as written in (3.3) and (3.5), both $\mathscr{PG}$ schemes miss a proper scaling with the physical viscosity ν of the ($\mathscr{RD}$ flavored) stabilization. This is achieved by introducing the modified test functions

$$\omega_i^*(x,y) = \psi_i(x,y) + \xi(Pe)\, s_i(x,y) \tag{3.6}$$

and

$$\widetilde{\omega}_i^*(x,y) = \varphi_i(x,y) + \xi(Pe)\,\widetilde{s}_i(x,y) \tag{3.7}$$

with $\xi(Pe)$ a properly defined continuous function of the local Peclet number, such that

$$\lim_{Pe\to 0}\xi(Pe)=0 \quad \text{and} \quad \lim_{Pe\to\infty}\xi(Pe)=1.$$

Finally, we introduce two families of *hybrid $\mathscr{RD}$–$\mathscr{PG}$* schemes which, in the limit of pure advection, reduce to the fluctuation schemes of [1], and have uniform accuracy properties.

*Scheme $\mathscr{RD}^1(P^2)$-LDA**: With the notation of Section 1, we first consider the schemes given by (1.2) with

$$\Psi_i^{T_s}=\Psi_i^{\mathrm{G}}+\xi(Pe)(\beta_i\phi^{T_s}-\Psi_i^{\mathrm{G}})+\int_{T_s}\nu\nabla\omega_i^*\cdot\nabla u_h\,\mathrm{d}x\,\mathrm{d}y, \quad \Psi_i^{\mathrm{G}}=\int_{T_s}\psi_i\vec{a}\cdot\nabla u_h\,\mathrm{d}x\,\mathrm{d}y. \tag{3.8}$$

Note that in general for (3.8) $\Psi_i^{T_s}\neq 0\ \forall T_s\in T$, whenever $i\in T$. Last expression shows the main idea behind our approach: *the $\mathscr{RD}$ discretization of the advective operator is used to stabilize the Galerkin scheme defined by Ψ_i^G*. Consistency with the discrete diffusion operator is achieved by a proper definition of $\xi(Pe)$ and ω_i^*. In particular, in the sub-elements that do not contain node i, one simply has $\beta_i=0$. This fact is already accounted for in the definition of ω_i^* which verifies on all $T_s\in T$:

$$\frac{1}{|T_s|}\int_{T_s}\omega_i^*\,\mathrm{d}x\,\mathrm{d}y=\xi(Pe)\beta_i+(1-\xi(Pe))\frac{1}{|T_s|}\int_{T_s}\psi_i\,\mathrm{d}x\,\mathrm{d}y. \tag{3.9}$$

*Scheme $\mathscr{RD}^2(P^2)$-LDA**: We consider the compact hybrid $\mathscr{RD}$–$\mathscr{PG}$ scheme for which $\Psi_i^{T_s}=0$ if $i\notin T_s$, otherwise

$$\Psi_i^{T_s}=\Psi_i^{\mathrm{C}}+\xi(Pe)(\beta_i\phi^{T_s}-\Psi_i^{\mathrm{C}})+\int_{T_s}\nu\nabla\widetilde{\omega}_i^*\cdot\nabla u_h\,\mathrm{d}x\,\mathrm{d}y, \quad \Psi_i^{\mathrm{C}}=\int_{T_s}\varphi_i\vec{a}\cdot\nabla u_h\,\mathrm{d}x\,\mathrm{d}y. \tag{3.10}$$

In this case, *the $\mathscr{RD}$ discretization of the advective operator is used to stabilize the centered scheme defined by Ψ_i^C*. Consistency with the discrete diffusion operator is achieved by a proper definition of $\xi(Pe)$ and $\widetilde{\omega}_i^*$. In particular, as (3.8), the more efficient discretization defined by (3.10) enjoys the property

$$\frac{1}{|T_s|}\int_{T_s}\widetilde{\omega}_i^*\,\mathrm{d}x\,\mathrm{d}y=\xi(Pe)\beta_i+(1-\xi(Pe))\frac{1}{|T_s|}\int_{T_s}\varphi_i\,\mathrm{d}x\,\mathrm{d}y=\beta_i^* \tag{3.11}$$

with β_i^* as in Eq. (2.5).

4. Numerical experiments on P^2 elements

We present a grid convergence study on the problem of Section 2.1 using a P^2 interpolation. As before, we discuss the convergence of the L^2 norm of the error when h is reduced. The study is performed on a set of irregular Weatherhill meshes. We use as underlying $\mathscr{RD}$ scheme the LDA defined on each sub-element by the distribution coefficient (2.6), with the normals computed locally, based on the geometry of the sub-triangle (see [1] for more). For the test functions ω_i^* the $\alpha_i^{T_s}$ coefficients needed for the evaluation of the stabilization terms are analytically computed by imposing (3.9) (or equivalently (3.2)). In all the computations we have set

$$\xi(Pe)=\max(0,1-1/Pe).$$

We refer to [7] for a study of different definitions of this parameter. The results reported have been obtained for $\nu=0.01$. The behavior observed for values of ν from 10^{-6} to 1 is the same. On the left pictures in Figs. 6–9 we report the grid convergence histories of the $\mathscr{PG}$ Scheme (3.3) and of the consistent variant obtained using the test function (3.6) (denoted as $\mathscr{PG}^1(P^2)$-LDA and $\mathscr{PG}^1(P^2)$-LDA*), of the $\mathscr{PG}$ Scheme (3.5) and of the consistent variant obtained using the test function (3.7) (denoted as $\mathscr{PG}^2(P^2)$-LDA and $\mathscr{PG}^2(P^2)$-LDA*), of the hybrid Scheme (3.8) and of the inconsistent variant obtained for $\xi(Pe)=1$ (denoted as $\mathscr{RD}^1(P^2)$-LDA* and $\mathscr{RD}^1(P^2)$-LDA), and of the hybrid Scheme (3.10) and of the inconsistent variant obtained for $\xi(Pe)=1$ ($\mathscr{RD}^2(P^2)$-LDA* and $\mathscr{RD}^2(P^2)$-LDA). All the results have been obtained using the explicit iterative procedure (1.2).

When the scaling function $\xi(Pe)$ is not introduced (or equivalently if $\xi(Pe)=1$), third-order accuracy is not achieved, despite the P^2 variable representation. Conversely, when the upwind stabilization is properly scaled, all the schemes

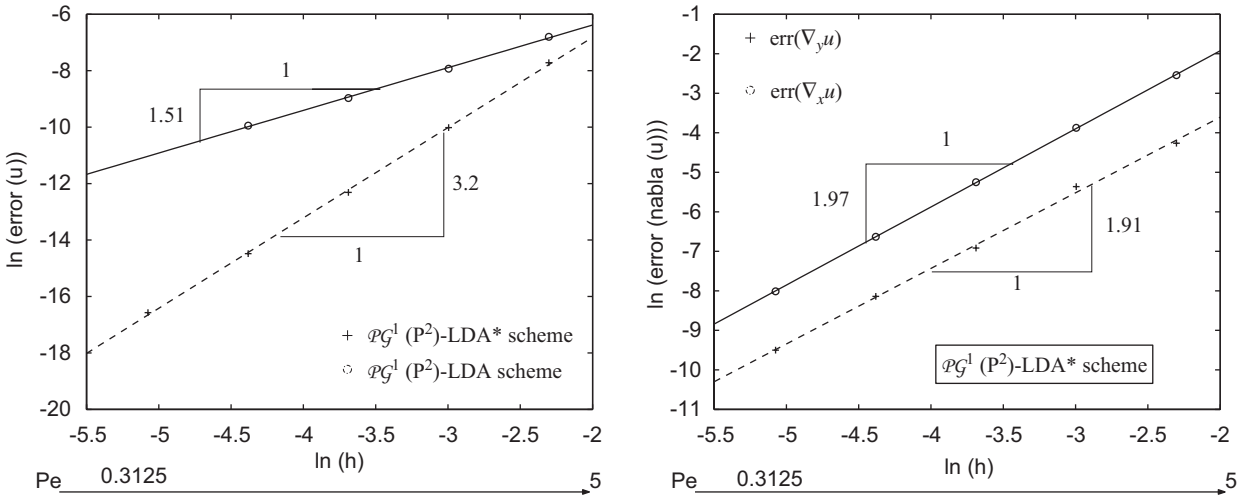

Fig. 6. Grid convergence study: $\nu = 0.01$. Error in terms of u (left) and of ∇u (right).

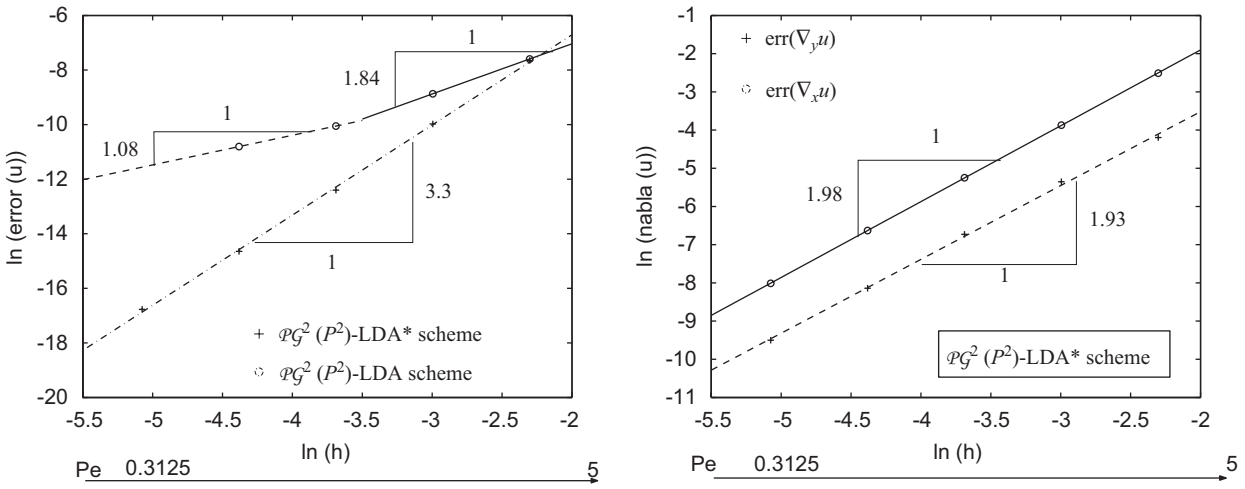

Fig. 7. Grid convergence study: $\nu = 0.01$. Error in terms of u (left) and of ∇u (right).

show the expected accuracy, and, moreover, they yield a uniform second-order approximation of the gradient of the solution, as shown in the right pictures in Figs. 6–9. If this is not very surprising for the $\mathcal{PG}$ schemes based on the *more traditional* formulation (3.3), it is very interesting for both the compact $\mathcal{PG}$ (3.5) and for the hybrid schemes. The compact hybrid Scheme (3.10) represents a very good candidate to generalize the fluctuation schemes of [1] to advective–diffusive problems. Compared to the schemes proposed in [5], the ones discussed here are far more efficient, due to the use of the variational formulation. Note also, that the *blending* used to define the hybrid schemes only involves the evaluation of one extra sum with respect to a $\mathcal{PG}$ scheme, due to the relations

$$\phi^{T_s} = \int_{T_s} \vec{a} \cdot \nabla u_h \, \mathrm{d}x \, \mathrm{d}y = \sum_{j \in T_s} \int_{T_s} \varphi_j \vec{a} \cdot \nabla u_h \, \mathrm{d}x \, \mathrm{d}y = \sum_{j \in T} \int_{T_s} \psi_j \vec{a} \cdot \nabla u_h \, \mathrm{d}x \, \mathrm{d}y.$$

It is very interesting to look at the efficiency of the very high-order discretization we propose. To this end, denoting the norm of the error by ε, we define the following efficiency monitors:

$$\eta_1 = \frac{1}{(\#\text{operations per iteration}) \times \varepsilon}, \quad \eta_2 = \frac{1}{(\#\text{operations per iteration}) \times (\#\text{iterations}) \times \varepsilon}.$$

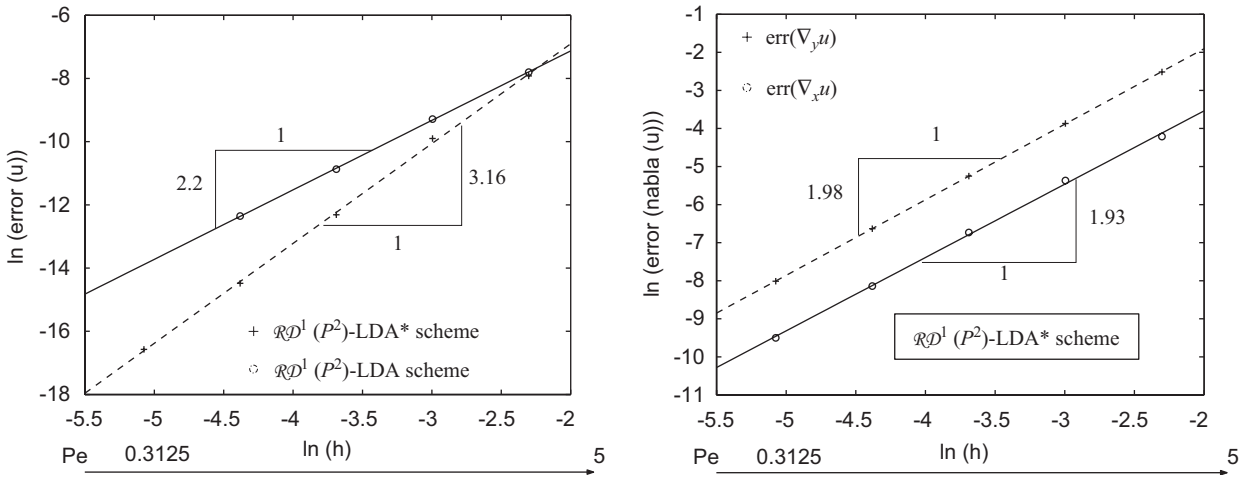

Fig. 8. Grid convergence study: $\nu = 0.01$. Error in terms of u (left) and of ∇u (right).

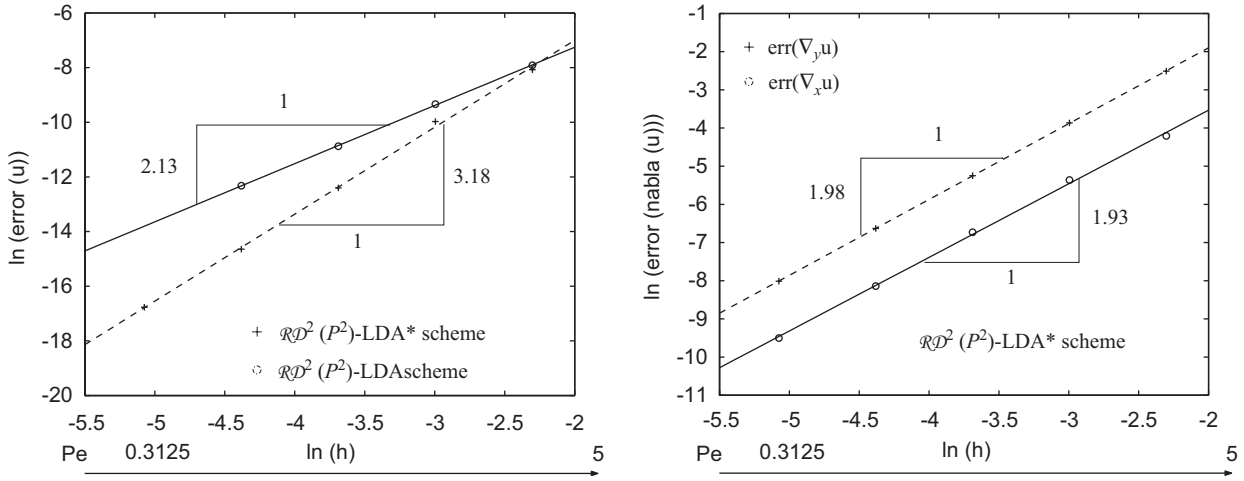

Fig. 9. Grid convergence study: $\nu = 0.01$. Error in terms of u (left) and of ∇u (right).

We are then interested in the ratios

$$R_1 = \frac{\eta_1^{P^2}}{\eta_1^{P^1}} \quad \text{and} \quad R_2 = \frac{\eta_2^{P^2}}{\eta_2^{P^1}}.$$

The advantage of the use of the very high-order schemes is measured by how much R_1 and R_2 exceed the unity. In general, R_2 is a more honest efficiency monitor. We also report the values of R_1, which are not affected by the inefficiency of the iterative procedure (1.2). Basically, the values of R_1 are the ones one would obtain at fixed number of iterations, when going from P^1 to P^2 interpolation. For most of our results, this is a realistic monitor, and it would be in general if an efficient solution strategy would be adopted. In Tables 1 to 4, we report errors, number of iterations and efficiency ratios for all the high-order schemes tested in the grid convergence study. The P^1 results used for comparison are obtained on the meshes composed by all the sub-elements. Hence, the comparison is performed at fixed number of degrees of freedom. The tables show that the very high-order schemes are more efficient than the second-order one. This is especially true on finer meshes, due to the fast error reduction obtained with the third-order discretization. The schemes based on the compact test functions are roughly twice more efficient.

Table 1
Efficiency of the $\mathscr{PG}^1(P^2)$-LDA*: $\nu = 0.01$

h	ε_{P^1}	# Iteration(P^1)	ε_{P^2}	# Iteration(P^2)	R_1	R_2
0.05	2.88e −03	269	4.44e −04	124	0.81	1.75
0.025	7.11e −04	611	4.47e −05	430	1.98	2.82
0.0125	1.86e −04	1591	4.50e −06	2240	5.17	3.66
0.00625	2.76e −5	4972	5.13e −07	7295	6.72	4.58
0.003125	9.97e −6	17 470	6.34e −8	28 250	19.65	12.15

Table 2
Efficiency of the $\mathscr{PG}^2(P^2)$-LDA*: $\nu = 0.01$

h	ε_{P^1}	# Iteration(P^1)	ε_{P^2}	# Iteration(P^2)	R_1	R_2
0.05	2.88e −03	269	4.76e −04	102	1.51	5.05
0.025	7.11e −04	611	4.64e −05	359	3.83	6.51
0.0125	1.86e −04	1591	4.11e −06	2210	11.31	8.14
0.00625	2.76e −5	4972	4.37e −7	4292	15.78	8.29
0.003125	9.97e −6	17 470	5.20e −8	28 376	47.93	29.51

Table 3
Efficiency of the $\mathscr{RD}^1(P^2)$-LDA*: $\nu = 0.01$

h	ε_{P^1}	# Iteration(P^1)	ε_{P^2}	# Iteration(P^2)	R_1	R_2
0.05	2.88e −3	269	3.63e −4	168	1.19	1.9
0.025	7.11e −04	611	5.01e −5	388	2.12	3.35
0.0125	1.86e −04	1591	4.49e −06	2231	6.21	4.43
0.00625	2.75e −5	4972	5.12e −7	7295	8.062	5.49
0.003125	9.97e −6	17 470	6.34e −8	28 250	23.59	14.59

Table 4
Efficiency of the $\mathscr{RD}^2(P^2)$-LDA*: $\nu = 0.01$

h	ε_{P^1}	# Iteration(P^1)	ε_{P^2}	# Iteration(P^2)	R_1	R_2
0.05	2.88e −03	269	3.31e −04	104	2.17	5.63
0.025	7.11e −04	611	4.67e −05	403	3.81	5.77
0.0125	1.86e −04	1591	4.1e −06	2158	11.34	8.36
0.00625	2.75e −5	4972	4.37e −07	4150	15.73	18.84
0.003125	9.97e −6	17 470	5.19e −8	28 376	48.02	29.57

5. Conclusion

We have discussed preliminary results on the construction of high-order fluctuation schemes [1] for advection–diffusion. First, a variational formulation of second-order $\mathscr{RD}$ schemes has been introduced. As in streamline upwind FE, a correct scaling of the upwind $\mathscr{RD}$ stabilization with a cell Peclet number has been shown to be fundamental to achieve uniform second-order accuracy. Generalizations to higher order have been discussed. As in the P^1 case, the basic idea is to use the $\mathscr{RD}$ discretization of the advection operator to stabilize a central discretization. The correct coupling between discrete advection and discrete diffusion operators is guaranteed by a hybrid $\mathscr{RD}$– $\mathscr{PG}$ formulation, and by a proper scaling of the $\mathscr{RD}$ stabilization with a cell Peclet number. Numerical results for third-order schemes confirm the expected uniform accuracy. More work is certainly needed to give a general theoretical basis for the analysis of the schemes.

Acknowledgment

This work was performed when the first author was still member of the Doctoral programme of the von Karman Institute for Fluid Dynamics.

References

[1] R. Abgrall, P.L. Roe, High-order fluctuation schemes on triangular meshes, J. Sci. Comput. 19 (2003) 3–36.
[2] H. Deconinck, R. Abgrall, Introduction to Residual Distribution Methods, in: 34th CFD Course: Higher-order Discretization Methods, VKI LS 2006-01, von Karman Institute for Fluid Dynamics, Belgium, 2005.
[3] L.P. Franca, S.L. Prey, T.J.R. Hughes, Stabilized finite element methods:I. Application to the advective-diffusive model, Comput. Methods Appl. Mech. Eng. 95 (1992) 253–276.
[4] T.J.R. Hughes, A. Brook, Streamline upwind Petrov–Galerkin formulations for convection dominated flows with particular emphasis on the incompressible Navier–Stokes equations, Comput. Methods Appl. Mech. Eng. 32 (1982) 199–259.
[5] H. Nishikawa, P.L. Roe, On high-order fluctuation splitting schemes for Navier–Stokes equations, in: ICCFD3, Third International Conference on Computational Fluid Dynamics, Springer, Berlin, 2004.
[6] H. Paillère, J. Boxho, G. Degrez, H. Deconinck, Multidimensional upwind residual distribution schemes for the convection-diffusion equation, Int. J. Numer. Methods Fluids 23 (1996) 923–936.
[7] M. Ricchiuto, N. Villedieu, R. Abgrall, H. Deconinck, High-order residual distribution schemes: discontinuity capturing crosswind dissipation and extension to advection–diffusion, in: 34th CFD Course: Higher-order Discretization Methods, VKI LS 2006-01, von Karman Institute for Fluid Dynamics, Belgium, 2005.